Journal of Statistical Pysics, Vol. 70, Nos. 3/4, 1993

Incommensurate Structure in the Lattice-Gas ANNNI Model

Iva Karasová[1] **and Anton Šurda**[1]

Received January 16, 1992; final August 3, 1992

The phase diagram of the two-dimensional lattice-gas ANNNI model is investigated using the cluster transfer-matrix method. The numerical calculations have shown commensurate, disordered, and floating incommensurate phases. The properties of the incommensurate phase are studied in detail and the position of the Lifshitz point is discussed.

KEY WORDS: Lattice-gas ANNNI model; floating incommensurate phase; spatially modulated structures.

1. INTRODUCTION

Recently a generalized mean-field method for the treatment of spatially modulated structures, including incommensurate ones, in the lattice models has been developed.[1] It was applied to a model with competing interactions simulating the ordering of oxygen atoms in the CuO_2 plane of an $YBa_2Cu_3O_{7-\delta}$ crystal.[2] A phase diagram with a set of commensurate structures and an incommensurate structure between them was obtained. A similar behavior, though with less numerous phases, is observed in a much simpler model—the axial-next-nearest-neighbor Ising (ANNNI) model,[3,4] which was extensively studied in the last decade. In three dimensions it displays an infinite hierarchy of commensurate structures; for two-dimensional models an area of a floating incommensurate structure appears in the phase diagram.

The cluster transfer-matrix method[1,2] describes successfully structures incommensurate to the underlying lattice, as it recasts the problem of calculation of the partition function to a nonlinear mapping procedure. In

[1] Institute of Physics, Slovak Academy of Science, Dúbravská cesta 9, 842 28 Bratislava, Czechoslovakia.

0022-4715/93/0200-0675$07.00/0

distinction to a similar idea of mapping the average row magnetization in the 3D ANNNI model exploited by Jensen and Bak,[5] the mapping procedure is applied to auxiliary functions $\Psi_{i,j}$ defined on finite clusters in the 2D ANNNI model. In the case of a semi-infinite crystal the initial values of the functions $\Psi_{i,j}$ represent boundary condition on the lattice surface. In the process of mapping, the bulk value of the $\Psi_{i,j}$ is obtained. Thus, the physical meaning of the procedure is transparent and it inherently converges to the physically stable or metastable solutions. The method yields the spatial dependence of the correlation functions and not only the wavelength of the incommensurate structure, as in the finite-size scaling transfer-matrix method.[6]

The ANNNI model has been widely studied by numerous authors and methods, including Monte Carlo simulations,[7–9] free and interacting fermion approximations,[10,11] interface calculations,[12] series analysis,[13] the cluster variation method,[14] the dynamical method,[15] and transfer-matrix analysis.[16]

The most important features of the resulting phase diagram are very similar in all the above-mentioned approaches. The most disputed points are the behavior of the system at low temperatures between the ferromagnetic and the commensurate modulated phases and the existence and position of the Lifshitz points. Both problems will be studied in the lattice-gas formulation in Section 4. First, in Section 2, we briefly describe the cluster transfer-matrix method used in the present paper. In Section 3, we apply this method to the lattice-gas analogue of the ANNNI model on the rectangular lattice.

Despite the fact that many of the approaches (Monte Carlo method,[7–9] free fermion method,[10] mean field approximation) show a direct phase transition line between the ferromagneric and the incommensurate phases, it is generally accepted that the disordered phase is stable down to the multiphase point at $T=0$, as a consequence of unbinding of dislocations in the floating phase. As our method does not describe wall dislocations, it predicts a Lifshitz point at the boundary of the ferromagnetic phase. Nevertheless it can serve as a good starting point for a theory of dislocations, as it may be used for the calculation of the wall and dislocation energies. The hint that the high-temperature phase persists to the low temperatures is discussed in Section 4.

There is no agreement upon the position of the Lifshitz point at the commensurate modulated phase boundary. Our calculation shows that the incommensurate phase exists in the vicinity of the commensurate phase up to the point where the nearest-neighbor interaction in the competing direction is equal to zero, i.e., where the ANNNI model decouples to two independent Ising models.

2. METHOD

The cluster transfer-matrix method has been applied to the ferromagnetic Ising model[1] and to a model of oxygen atoms with competing interactions,[2] and quite recently it was generalized to a description of quantum systems.[17] In this paper we present a simplified version of the method more appropriate for numerical calculation. From the beginning we assume that the system in thermal equilibrium may be spatially modulated.

The method is suitable for lattice models with short-range interactions, the Hamiltonians of which can be written in form of a sum of cluster Hamiltonians

$$H = \sum_{i=1}^{J} H_i(\{K_l\}; n_{i_1},..., n_{i_j}) \tag{1}$$

where i numbers lattice sites, n_{i_k} are site variables defined on a finite-size cluster of sites around the site i, and $n_j = 0, 1,..., N$. A set of short-range interaction constants is denoted by $\{K_l\}$. (In the case of the lattice-gas analogue of the ANNNI model, $N = 1$.)

In the first step of the calculation, it is convenient to consider rows perpendicular to the expected incommensurate structures and to express the Hamiltonian as a sum of strip Hamiltonians dependent on the row variables $N_i \equiv \{n_{i,1}, n_{i,2},..., n_{i,s}\}$, $s \to \infty$,

$$H = \sum_{i=1}^{M} G_i(\{K_l\}; N_i,..., N_{i+k}) \tag{2}$$

where k is the maximum interaction range in the direction perpendicular to the rows. (For the ANNNI model $k = 2$.) As each row appears in $k+1$ different strip Hamiltonians G_i, the short-range interactions may be divided among different strip Hamiltonians practically in an arbitrary way. On the other hand, our approximate approach will not reproduce the ground-state properties and the symmetries of the model for all choices of G_i.

In the ANNNI model the resulting magnetization is exactly equal to zero for the paramagnetic state in the case when in our method not only H but all G_i possess particle–hole symmetry as well. (For low temperatures, the magnetization may be nonzero due to the spontaneous symmetry breaking, which is a characteristic property of the method.) Similarly, for the ground state, the method yields the exact value of the phase transition between two different structures only if all the cluster energies G_i are equal in both phases at the phase transition point.

The exponential of the strip Hamiltonian G_i is usually called the

transfer matrix, despite the fact that it is a function of row variables N_j rather than a matrix,

$$T_i(N_i,..., N_{i+k}) = \exp[\beta G_i(\{K_l\}; N_i,..., N_{i+k})], \quad \beta = \frac{1}{T} \tag{3}$$

Using it, the calculation of the partition function

$$Z = \sum_{\{N_i\}} \exp[\beta H(n_i)]$$

can be performed step by step, by introducing auxiliary functions Ψ_i,

$$\sum_{N_i} \Psi_i(N_i,..., N_{i+k-1})\, T_i(N_i,..., N_{i+k}) = \lambda_i \Psi_{i+1}(N_{i+1},..., N_{i+k}) \tag{4}$$

If the functions Ψ_j are suitably normalized, the partition function is simply a product of all the constants λ_i,

$$Z = \prod_{i=1}^{M} \lambda_i$$

It follows from (1) that the strip Hamiltonians G_i can be expressed as a sum of cluster Hamiltonians along the strip. That implies factorization of their exponentials—the transfer matrices

$$T_i(N_i,..., N_{i+k}) = \prod_j T_{i,j}(M_{i,j}^{k,t}) \tag{5}$$

where $M_{i,j}^{k,t}$ represents the occupation numbers of a rectangular cluster of sites,

$$M_{i,j}^{k,t} \equiv \begin{pmatrix} n_{i,j} & \cdots & n_{i,j+t} \\ \vdots & \ddots & \vdots \\ n_{i+k,j} & \cdots & n_{i+k,j+t} \end{pmatrix} \tag{6}$$

The second index in (5) and (6) denotes the position of the site in the row.

The factorization of the T matrix is a consequence of the fact that in the system only short-range interactions are present. The auxiliary function Ψ_i represents the effect of indirect interactions between sites in one half-lattice mediated by the other half-lattice. Then, the factorization of Ψ_i would be equivalent to the assumption that these interactions are of short range. We shall see that after factorization of Ψ_i and Ψ_{i+1}, e.g.,

$$\Psi_i(N_i,..., N_{i+k-1}) \simeq \prod_j \Psi_{i,j}(M_{i,j}^{k-1,t}) \tag{7}$$

the iteration step (4), where a function of an infinite number of variables appears, can already be performed. The factorization (7) is the only approximation in our method and the values of k and t determine its order.

The cluster functions $\Psi_{i,j}$ in (7) may be determined from the requirement that the thermal averages of physical quantities defined on small clusters are not changed after factorization,

$$\begin{aligned}\langle A\rangle &= \sum_{N_i,\ldots,N_{i+k-1}} \Psi_i(N_i,\ldots,N_{i+k-1})\, A(M_{j,s}^{l,n})\, \tilde{\Psi}_{i+k-1}(N_i,\ldots,N_{i+k-1}) \\ &= \sum_{N_i,\ldots,N_{i+k-1}} \prod_n \Psi_{i,n} A \prod_m \tilde{\Psi}_{i+k-1,m} \qquad (8)\end{aligned}$$

where $i \leqslant j \leqslant i+k-1$, $j+l \leqslant i+k-1$, $n \leqslant t$, and the right-hand auxiliary function $\tilde{\Psi}$ is defined by an equation analogous to (4),

$$\begin{aligned}&\sum_{N_{i+k}} T_i(N_i,\ldots,N_{i+k})\, \tilde{\Psi}_{i+k}(N_{i+1},\ldots,N_{i+k}) \\ &\quad = \tilde{\lambda}_{i+k}\, \tilde{\Psi}_{i+k-1}(N_i,\ldots,N_{i+k-1}) \qquad (4')\end{aligned}$$

Equation (8) is satisfied if $\Psi_{i,j}$ (and similarly $\tilde{\Psi}_{i,j}$) is chosen as

$$\Psi_{i,j}(M_{i,j}^{k-1,t}) = \sum_{L_{ij}^{k-1,t}} \Psi_i \Big/ \sum_{L_{ij}^{k-1,t-1}} \Psi_i \qquad (9)$$

where we sum over site variables of infinite clusters of sites,

$$L_{ij}^{l,t} = (N_i,\ldots,N_{i+l}) - M_{i,j}^{l,t}$$

The choice of (7) is not unique. The cluster function $\Psi_{i,j}$ is determined up to an arbitrary multiplier and an inverse of the multiplier of the cluster function belonging to the next site,

$$\Psi_i = \prod_j U_j(M_{i,j}^{k-1,t-1})\, \Psi_{i,j}(M_{i,j}^{k-1,t})\, U_{j+1}^{-1}(M_{i,j+1}^{k-1,t-1})$$

For example, if $\Psi_{i,j}$ is given by (9) and

$$U_{j+1} = \left(\sum_{L_{i,j}^{k-1,t-1}} \Psi_i \right)^{-1/2}$$

the resulting function $U_j \Psi_{i,j} U_{j+1}^{-1}$ is symmetric with respect to the mirror reflection $i \leftrightarrow i+t$, etc., for spatially homogeneous functions Ψ_i.

After factorization, Eq. (4) can be reformulated directly in terms of functions $\Psi_{i,j}$ defined already on finite clusters. Combining (4) and (9), we get

$$\Psi_{i+1,m} = \sum_{L_{i+1,m}^{k-1,t}} \sum_{N_i} \prod_j \Psi_{i,j} T_{i,j} \Big/ \sum_{L_{i+1,m}^{k-1,t-1}} \sum_{N_i} \prod_j \Psi_{i,j} T_{i,j}$$

$$= \sum_{n_{i,m},\ldots,n_{i,m+t}} \sum_{L_{i+1,m}^{k,t}} \prod_j \Psi_{i,j} T_{i,j} \Big/ \sum_{n_{i,m},\ldots,n_{i,m+t}} \sum_{L_{i+1,m}^{k,t-1}} \prod_j \Psi_{i,j} T_{i,j} \quad (10)$$

Summation over infinite clusters $L_{i+1,m}^{k,t}$, $L_{i+1,m}^{k,t-1}$ can be done exactly using again the transfer-matrix technique. The transfer matrix $S_{i,j} = \Psi_{i,j} T_{i,j}$ of this one-dimensional problem is finite.

The iteration procedure (10) represents a nonlinear mapping $\Psi_{i,j} \to \Psi_{i+1,j}$ of the auxiliary functions $\Psi_{i,j}$ in the ith row onto the functions in the $(i+1)$th row. The function $\Psi_{i,j}$ in the process of iteration may converge to a homogeneous solution or oscillate among a finite number of values or acquire an infinite number of values in a quasiperiodic way. These possibilities correspond to homogeneous, commensurate, and incommensurate structures of the lattice, respectively. In other words, the spatial behavior of the functions $\Psi_{i,j}$ alone determines the phase diagram of the Hamiltonian H. We note that in the framework of the cluster transfer-matrix method we can calculate the correlation functions and the free energy, too.[1,2]

The functions $\Psi_{i,j}$ may also depend on the position along the strip j, but only a finite number of them are allowed to be different from each other. In the case of spatial modulation along the strips, we have to choose carefully the initial values of the auxiliary functions at the left and right ends of the strip when evaluating the sum in (10), to be consistent with resulting structures.

As stressed in the Introduction, the main difference between our nonlinear approach and that of Jensen and Bak[5] is that we map auxiliary functions $\Psi_{i,j}$ instead of mean occupation numbers $\langle n \rangle$. As a consequence we obtain stable fixed points and orbits, which can be found easily with high precision. The method is dimension sensitive.

3. LATTICE-GAS ANNNI MODEL

In this section our cluster approximation method is applied to the lattice-gas analogue of the 2D ANNNI model on the rectangular lattice. This model is described by the standard Hamiltonian

$$\beta H = \sum_{i,j} H_{i,j}$$

$$H_{i,j} = \mu n_{i,j} + n_{i,j}(K_0 n_{i,j+1} + K_1 n_{i+1,j} + K_2 n_{i+2,j}) \quad (11)$$

$$\mu = \frac{\mu_0}{T}, \qquad K_m = \frac{J_m}{T} \qquad (m = 0, 1, 2)$$

where i refers to the rows of the rectangular lattice and j specifies the sites in these rows. The chemical potential μ_0 is given by

$$\mu_0 = -J_0 - J_1 - J_2$$

which means that there is a zero magnetic field in the original ANNNI model. If the Hamiltonian (11) describes an adsorbate system, μ_0 must be read as $(\mu_0 + \varepsilon)$, where ε denotes the binding energy of the adatoms to the substrate. The $n_{i,j} = 0$ or 1 are the occupation numbers and for the pair interaction constants J_0, J_1, and J_2 a parametrization

$$J_1 = (1-\alpha) J_0, \qquad J_2 = -\alpha J_0, \qquad 0 \leqslant \alpha \leqslant 1$$

is chosen $(J_0 > 0)$.

As shown in the preceding section, the factorization (7) determines the order of the approximation in our method. Let us recall that the cluster $M_{i,j}^{k,t}$ has a rectangular shape with sides k and t lattice constants, respectively. In the case of the ANNNI model k is equal to two [the maximum interaction range in the Hamiltonian (11)] and t depends on our choice. Our calculations are performed for $t = 1$ and 2, i.e., we use a pair of the lowest approximations of our method. All the following expressions will be given in explicit form only for $t = 1$.

In order to solve the iteration equation (10), we need to express the transfer matrix elements $T_{i,j}$ by means of the parameters of the Hamiltonian (11). Comparing first (3) with (5), and then (2) with (11), we get the relation

$$T_{i,j}(M_{i,j}^{2,1}) = \exp[\beta G_{i,j}(M_{i,j}^{2,1})] \tag{12}$$

where the strip Hamiltonian elements $G_{i,j}$ can be chosen in the form

$$\begin{aligned} G_{i,j} = {} & \mu_1(n_{i,j} + n_{i,j+1}) + \mu_2(n_{i+1,j} + n_{i+1,j+1}) + \mu_3(n_{i+2,j} + n_{i+2,j+1}) \\ & + \kappa_0(n_{i,j}n_{i,j+1} + n_{i+1,j}n_{i+1,j+1} + n_{i+2,j}n_{i+2,j+1}) \\ & + \kappa_1[n_{i+1,j}(n_{i,j} + n_{i+2,j}) + n_{i+1,j+1}(n_{i,j+1} + n_{i+2,j+1})] \\ & + \kappa_2(n_{i,j}n_{i+2,j} + n_{i,j+1}n_{i+2,j+1}) \end{aligned} \tag{13}$$

When using only the translational symmetry of the system, we get for the parameters of $G_{i,j}$ the following relations:

$$2\mu_3 = \mu_0 - 2\mu_1 - 2\mu_2$$

and

$$\kappa_0 = \frac{J_0}{3}, \qquad \kappa_1 = \frac{1-\alpha}{4} J_0, \qquad \kappa_2 = -\frac{\alpha}{2} J_0$$

The parameters μ_1 and μ_2 are not arbitrary, but they must satisfy the relations

$$2\mu_1 = -\kappa_0 - \kappa_1 - \kappa_2, \qquad 2\mu_2 = -\kappa_0 - 2\kappa_1$$

as a consequence of the particle–hole symmetry of the strip Hamiltonian G_i. (It is easy to verify that $\mu_1 = \mu_3$.) Only in this case we obtain the correct position of the phase transition from the (4×1) to the homogeneous (1×1) phase at zero temperature.

Substituting now (12) into (10) with $G_{i,j}$ defined by (13), the numerical iteration procedure may start. In the case $t = 1$ the multisite functions $\Psi_{i,j}(M_{i,j}^{1,1})$ (which are homogeneous along the strips, i.e., independent of j) are defined on the rectangular cluster consisting of only four lattice sites. The initial values of the functions

$$\Psi_{0,j}\begin{pmatrix} 0 & 0 \\ 0 & 0 \end{pmatrix}, \quad \Psi_{0,j}\begin{pmatrix} 1 & 0 \\ 0 & 0 \end{pmatrix}, \ldots, \quad \Psi_{0,j}\begin{pmatrix} 1 & 1 \\ 1 & 1 \end{pmatrix}$$

simulate the boundary condition of the studied 2D system on a semi-infinite half-lattice (for details see refs. 1 and 2). For $t = 2$, the above clusters are one column larger.

4. RESULTS AND DISCUSSION

The iteration equation (10) has been solved numerically for all the site configurations of the clusters $M_{i,m}^{1,1}$ and $M_{i,m}^{1,2}$. Analyzing then the spatial behavior of the functions $\Psi_{i,m}$ calculated at different values of the temperature and α, we get the phase diagram of the Hamiltonian (11) depicted for $t = 1$ in Fig. 1.

In the ground state the system can be in one of two phases, homogeneous (1×1) structure (in the Ising language, ferromagnetic structure) or the (4×1) structure. At $\alpha = 1/3$, the cluster energies $G_{i,j}$ of (13) and the Hamiltonian H of (11) of both structures are equal to each other, i.e., this point corresponds to the phase transition between these structures.

As expected, with increasing temperature $T_{\text{red}} = 4T/J_0$, besides commensurate structures, the floating incommensurate and disordered structures have been found as well. The calculated transition lines corresponding to the melting of commensurate structures ((1×1), (4×1)) are in relatively good agreement with the transition lines obtained by the interface free energy method[19] if the interfaces—as for our strips—are considered perpendicular to the competing interactions (in Fig. 1 the two-dot/dashed line[7] and the dotted line[20]).

As in Monte Carlo calculations,[7,8] our method exhibits a Lifshitz point on the (1×1) side of the phase diagram ($\alpha_L = 0.308$, $T_{\text{red},L} = 0.896$). However, the existence of this point at the boundary of the (1×1) phase

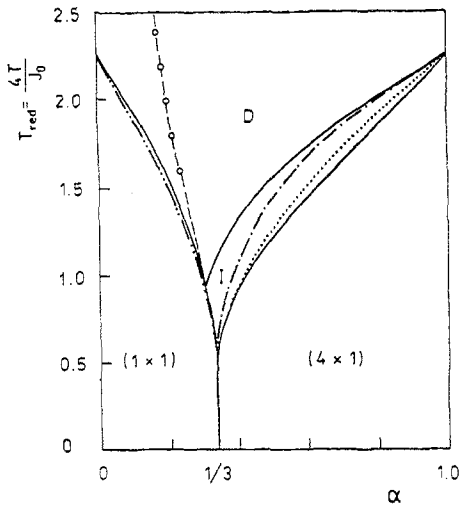

Fig. 1. Phase diagram calculated by means of the iteration procedure (10). Full lines represent the phase transitions between the commensurate [(1×1) and (4×1)], disordered (D), and floating incommensurate (I) structures. The dashed line represents the disorder line. The other transition lines are analytical results obtained by different authors using the interface method of Müller-Hartmann and Zittartz.[19] These correspond to the melting of the (1×1) structure (the two-dot/dashed line, Hornreich *et al.*[7]) and the (4×1) structure (the dotted line, Ala-Nissila *et al.*[20]; the dot-dashed line, Kroemer and Pesch[12]), respectively.

was questioned by Villain and Bak[10] and Coppersmith *et al.*[18] In their papers the important role of the dislocations was shown—the dislocations are not taken into consideration in our method. In addition, the Monte Carlo simulations[9] demonstrate strong finite-size effects, and ref. 9 also corrects the conclusion of the previous Monte Carlo calculations[7,8] as concerns the location of a Lifshitz point.

For $\alpha_L < \alpha < 1/3$, the (1×1) structure melts directly into the floating incommensurate phase.

For $\alpha > 1/3$, our numerical calculations show that in the studied model there are no direct transitions from the (4×1) structure into the disordered phase, i.e., the floating incommensurate phase extends up to $\alpha = 1$. (In the Ising model language this point corresponds to the reduction of the lattice into two independent Onsager lattices.) On the basis of these calculations it seems that in the ANNNI model, if the α-parametrization is used, there is no Lifshitz point on the (4×1) side of the phase diagram because the disordered, the floating incommensurate, and the (4×1) phases meet only at the decoupling point $\alpha = 1$ (our higher-order calculations for $t = 2$ have confirmed this conclusion). Similar behavior was obtained by Finel and de Fontaine[14] studying the instability of the disordered phase in the vicinity

of $\alpha = 1$. However, the precision of T^c calculated by them is only 25% for $\alpha = 1$; nevertheless, it is very good for $\alpha = 0$. Our approach yields very good results for $T^c_{\text{red}}(\alpha = 0) = 2.2694$ as well as for $T^c_{\text{red}}(\alpha = 1) = 2.272$. The exact value of the critical transition temperature[3] is $T^c_{\text{red}} = 2/\ln(\sqrt{2}+1) = 2.26918...$ for both $\alpha = 1$ and $\alpha = 0$. (The latter case corresponds to the classical Onsager lattice.) Note that the existance of the Lifshitz point on this side of the phase diagram has been discussed by many authors, but without concrete calculations (ref. 3 corrects the previous work of Selke[9]) and mostly within the κ parametrization, where κ is the competing parameter [$\kappa = J_2/J_1 > 0$; compare with Eq. (11)]. One assumes that the Lifshitz point occurs at $\kappa \to \infty$.

The shape of our phase diagram is very similar to that obtained by Finel and de Fontaine[14]—in particular its low-temperature part with the incommensurate phase is also present at $\alpha < 1/3$, with, however, a Lifshitz point. (An invisibly narrow area of the disordered phase stable to the multiphase point $T = 0$ is claimed in ref. 14.)

Motivated by the Monte Carlo simulations,[9] we also solved the iteration equation (10) for a (1×2) rectangular cluster having six lattice sites, i.e., using a higher-order approximation with $t = 2$. The results confirm the expected size effects; nevertheless, the characteristic features of the phase diagram—as shown by Fig. 1—are preserved. The boundary lines of the (1×1) and (4×1) structures are slightly shifted in the direction of the values obtained by the interface method of Müller-Hartmann and Zittartz[7,20], while the boundary between the floating and disordered phases is shifted to the lower values of T_{red}. The Lifshitz point has been detected at ($\alpha_L^{t=2} = 0.310$, $T^{t=2}_{\text{red,L}} = 0.859$), i.e., the value of T_{red} corresponding to the Lifshitz point decreases. Therefore, we can speculate that the increasing order of the approximation should shift the Lifshitz point along the boundary of the (1×1) phase to ($\alpha = 1/3$, $T_{\text{red}} = 0$).

The conjecture of the location of the Lifshitz point at ($\alpha = 1/3$, $T_{\text{red}} = 0$) might also be confirmed by the existence of metastable disordered solutions of Eq. (10) in a narrow region around $\alpha = 1/3$ up to $T_{\text{red}} = 0$. This solution has a higher free energy than the stable (1×1), floating incommensurate, and (4×1) phases. (The free energy has been calculated using the corresponding formulas in refs. 1 and 2.)

In the following part of this section we present the results of the iteration procedure (10) to illustrate the different structures of the phase diagram in Fig. 1. For this task it is convenient to choose[1,2] the effective chemical potential μ_i^{eff} simulating single-site effective interactions

$$\mu_i^{\text{eff}} = \log \Psi_{i,m}\begin{pmatrix} 1 & 0 \\ 0 & 0 \end{pmatrix} + \log \Psi_{i,m}\begin{pmatrix} 0 & 1 \\ 0 & 0 \end{pmatrix} - 2 \log \Psi_{i,m}\begin{pmatrix} 0 & 0 \\ 0 & 0 \end{pmatrix}$$

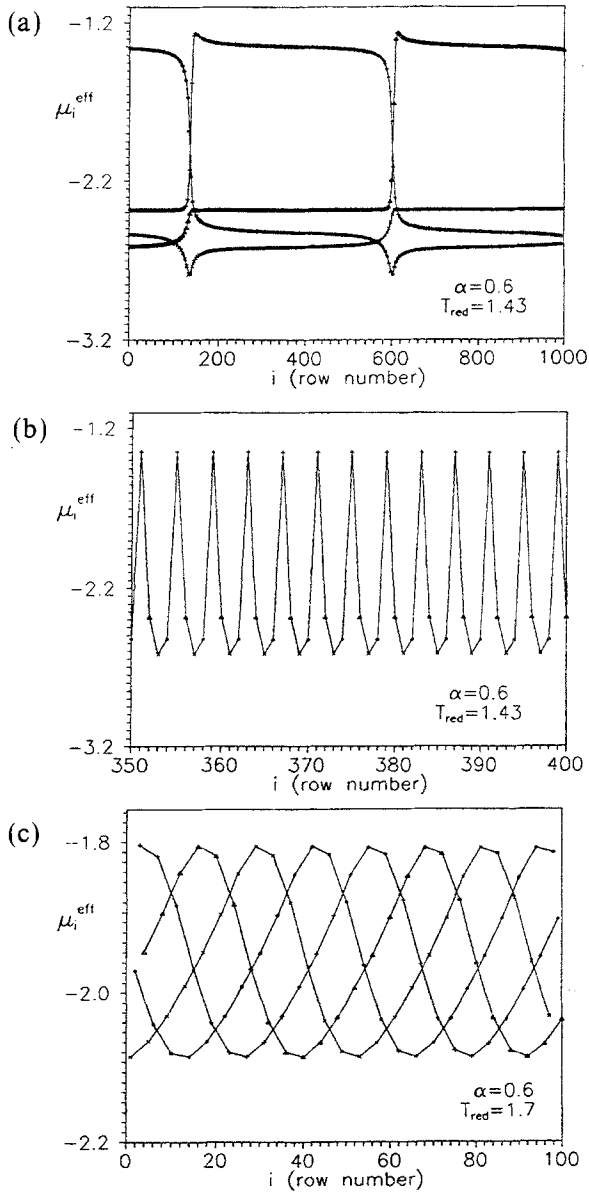

Fig. 2. The spatial dependence of the effective chemical potential μ_i^{eff} in the floating incommensurate phase [each fourth step is connected by a line and denoted by different symbol in order to see the structure of the results of the iteration procedure (10)] for $\alpha = 0.6$ and for (a) $T_{\text{red}} = 1.43$, i.e., slightly above the (4×1) structure; (b) detail of (a), where, in distinction to (a), the successive steps of (10) are connected to show the oscillation form of μ_i^{eff}; (c) $T_{\text{red}} = 1.7$, i.e., close to the boundary with the disordered phase.

instead of the individual functions $\Psi_{i,m}$. Iterating (10), we see that in our model the effective chemical potential μ_i^{eff} of the (4×1) structure oscillates among four values, while in the homogeneous (1×1) phase μ_i^{eff} converges (without any oscillations) to one of two values, depending on the initial boundary conditions.

The incommensurate phase is characterized by a quasiperiodic and oscillating behavior of μ_i^{eff}. Its concrete structure is determined by the temperature and the "competing" parameter α. The typical behavior of the effective chemical potential μ_i^{eff} in different parts of the incommensurate region is presented in Figs. 2 and 3. The region close to the (4×1) structure is shown in Fig. 2a. Here $\alpha = 0.6$, but in fact, at arbitrary α near the boundary of the (4×1) structure, the instability of the commensurate structure with respect to the formation of walls occurs. We see that the domain walls separate the commensurate areas formed by the (4×1) structure shifted with respect to each other by one lattice constant (practically horizontal parts of the curves; cf. Fig. 2a and Fig. 2b). The distance between the walls depends on the temperature and α (see below). A similar situation occurs near the boundary of the incommensurate region with the homogeneous (1×1) structure, as shown in Fig. 3. Here, however, the incommensurate structure consist of empty and full (1×1) structures (a consequence of the particle–hole symmetry). In this case the space dependence of the coverage inside the wall has the form of a kink. The situation in the upper part of the incommensurate region—close to the transition line into the disordered phase—is illustrated in Fig. 2c. For this region a sinusoidal shape of μ_i^{eff} is characteristic.

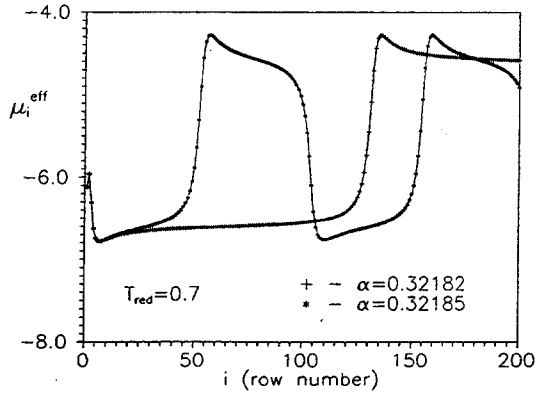

Fig. 3. The spatial dependence of the effective chemical potential μ_i^{eff} in the floating incommensurate phase close to the boundary of the homogeneous (1×1) structure (the successive steps are connected). For comparison the μ_i^{eff} for two different values of α are depicted.

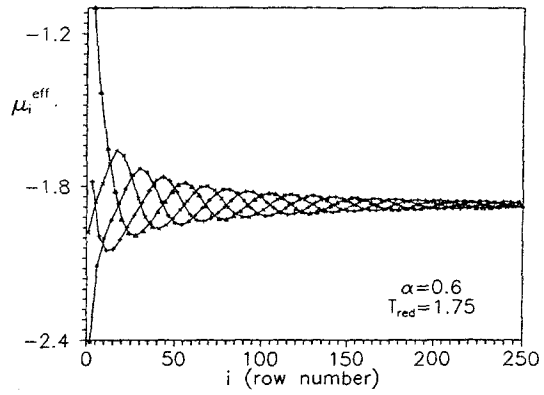

Fig. 4. The behavior of the effective chemical potential μ_i^{eff} in the disordered phase near the boundary of the floating incommensurate phase (each fourth step is connected).

The disordered phase is divided into two parts with different modulation regimes by a disorder line. It seems that this disorder line is tangential to the (1×1) phase boundary in the vicinity of the Lifshitz point $\alpha = \alpha_L$. (In Fig. 1 the calculated points of the disorder line are denoted by the open circles.) To the right of the disorder line, any disturbance of the disordered phase is followed by slowly decaying oscillations of μ_i^{eff} as shown in Fig. 4. To the left of the disorder line, the disturbances decay (monotonically) without oscillations. In both modulation regimes μ_i^{eff} converges to a single value.

To describe the incommensurate structure, it is useful to introduce the density q defined as $q = 1/l$, where l is the periodicity of the incommen-

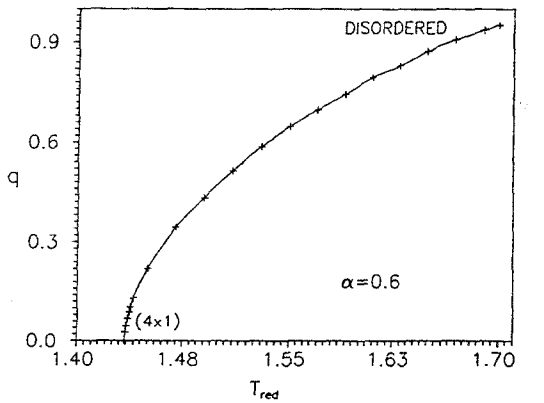

Fig. 5. The dependence of the density q on the temperature T_{red} in the region between the commensurate (4×1) structure and the disordered phase (for the same α as in Fig. 2).

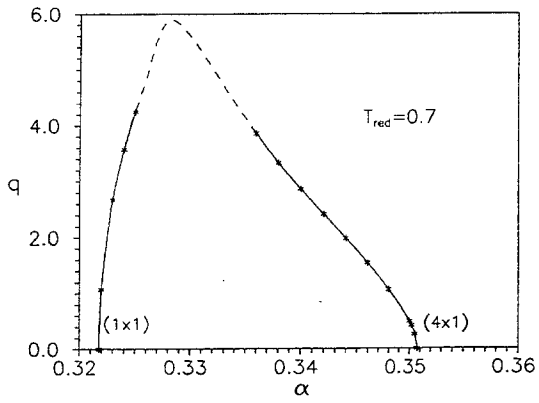

Fig. 6. The density q in the floating incommensurate phase between the (1×1) and (4×1) phases.

surate structure. For the region close to the (4×1) phase, $q = q_w/4$, where q_w is the wall density. The dependence of the density q on temperature is shown in Fig. 5. We see that the density q increases with the temperature. Near the boundary with the ordered (4×1) structure the temperature dependence of the density q is approximately $q \sim (T_{red} - T^c_{red})^{0.507}$. This result is in good agreement with the theory of Pokrovskii and Talapov,[21] which gives a square-root singularity. A similar behavior has been found for the α dependence of the density q. Figure 6 shows the density in the region between two commensurate phases. For $0.326 < \alpha < 0.336$ the q is determined with great inaccuracy (the dashed line), as here the "four curves" (see Fig. 2a) are transformed into "one curve" (see Fig. 3).

In conclusion, a recently developed method has been applied to the lattice-gas analogue of the ANNNI model. Its ability to describe the incommensurate phase in detail has been shown. The obtained phase diagram is in agreement with other approaches, but similarly as there, the theory of dislocations[10,18] and more detailed finite-size considerations[9] should be incorporated in the theory to get the correct low-temperature behavior.

REFERENCES

1. A. Šurda, *Phys. Rev. B* **43**:908 (1991).
2. A. Šurda, *Physica A* **178**:332 (1991).
3. W. Selke, *Phys. Rep.* **170**:213 (1988).
4. P. Bak, *Rep. Prog. Phys.* **45**:587 (1982).
5. M. H. Jensen and P. Bak, *Phys. Rev. B* **27**:6853 (1983).
6. P. D. Beale, P. M. Duxbury, and J. Yeomas, *Phys. Rev. B* **31**:7166 (1985).
7. R. M. Hornreich, R. Liebmann, H. G. Schuster, and W. Selke, *Z. Phys. B* **35**:91 (1979).

8. W. Selke and M. E. Fischer, *Z. Phys. B* **40**:71 (1980).
9. W. Selke, *Z. Phys. B* **43**:335 (1981).
10. J. Villain and P. Bak, *J. Phys.* (Paris) **42**:657 (1981).
11. M. D. Grynberg and H. Ceva, *Phys. Rev. B* **43**:13630 (1991).
12. J. Kroemer and W. Pesch, *J. Phys. A* **15**:L25 (1982).
13. M. E. Fisher and W. Selke, *Phil. Trans. R. Soc. A* **302**:1 (1981).
14. A. Finel and D. de Fontaine, *J. Stat. Phys.* **43**:645 (1986).
15. M. N. Barber and B. Derrida, *J. Stat. Phys.* **51**:877 (1988).
16. W. Pesch and J. Kroemer, *Z. Phys. B* **59**:317 (1985).
17. A. Šurda, to be published.
18. S. N. Coppersmith, D. S. Fisher, B. I. Halperin, P. A. Lee, and W. F. Brinkman, *Phys. Rev. Lett.* **46**:549 (1981).
19. E. Müller-Hartmann and J. Zittartz, *Z. Phys. B* **27**:261 (1977).
20. T. Ala-Nissila, J. Amar, and J. D. Gunton, *J. Phys. A* **19**:L41 (1986).
21. V. L. Pokrovskii and A. L. Talapov, *Zh. Eksp. Teor. Fiz.* **75**:1151 (1978).